

Design and Synthesis of NiO@Co₃O₄@ZSM-5 Heterogeneous Multitask Hollow Structures for Tandem Catalysis

Muhammad Waqas[✉]

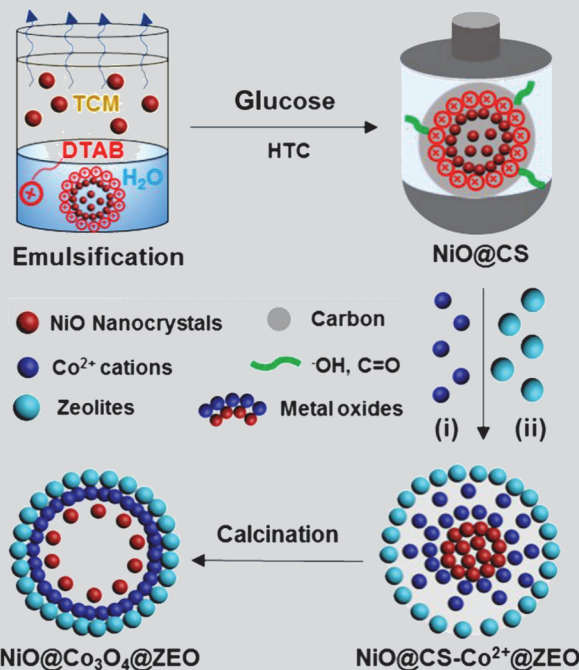
Received March 4, 2024

Accepted April 20, 2024

© Jilin University, The Editorial Department of Chemical Research in Chinese Universities and Springer-Verlag GmbH

Precipitation and impregnation procedures unevenly distribute metals on zeolite, limiting chemical transformation in Lewis-acid, Brønsted-acid and metal-catalyzed tandem reactions. Although, heterogeneous multitask transition metals oxides@zeolites are promising catalysts for sustainable processes; nevertheless, synthesis is fascinating and complex. Herein, the construction of purposely designed multitask materials segregated in selective shells reveals the remarkable spatial organization of metals-zeolite, resulting in them being suitable for a wide range of tandem reactions. The synthesis of multi-site catalysts begins with a universal wet chemistry approach that yields nickel oxide (NiO) crystals. Then, the NiO crystals are stabilized using cationic dodecyltrimethylammonium bromide, followed by achieving cross-linking carbon growth by emulsion polymerization of glucose in hydrothermal treatment to yield uniformed NiO@carbon spheres (NiO@CSs). Next, sequential adsorption of cobalt cations and colloidal ZSM-5 (1% in H₂O, mass fraction), followed by calcination in air, yielded NiO@cobalt oxide@zeolite denoted as NiO@Co₃O₄@ZEO hollow spheres. The hollowing mechanism and materials segregation within shells are revealed by scanning and transmission electron microscopy, thermogravimetric analysis, and X-ray diffraction. The finding advances the rational synthesis of heterogenous core-shell hollow structures for various gas phase catalytic tandem reactions to yield

valuable chemicals.



Keywords Multifunctional; Core-shell hollow spheres; Gas-phase reaction; Valuable chemical

1 Introduction

Synthesizing hollow materials with the required chemical composition and a clearly defined hierarchical architecture is the cornerstone of modern functional material science and cutting-edge technology.^[1–3] It also strengthens the structure-performance relationship.^[4–6] The integration of well-structured functional materials in shells is a classic example where reactivity originates from the material structure and traverses from the atomic scale to the microscale dimension, as well as from the spatial arrangement of components within composite shells.^[7,8]

Previously, significant efforts were devoted to synthesizing functional mixed metal oxides core-shell and multi-shelled hollow structures typically TiO₂/Fe₂TiO₅,^[9] TiN,^[10] BaTiO₃/TiO₂@polypyrrole,^[11] TiO₂/MAPbI₃,^[12] La-Rh@SrTiO₃,^[13] and LaCo_{1-x}Ni_xO_{3-x},^[14] Fe single atom doped MoS₂,^[15] FeS₂ hollow spheres,^[16] etc. Such a material design is an excellent strategy for solar water oxidation reactions, hydrogen evolution reactions, solar CO₂ evolution, or as an anode material in lithium-sodium ion batteries. The material attributes have special features, such as a high specific surface area that provides more active sites for reaction, excellent solar photon harvesting ability, a hollow interior that provides extra volume for reactant species recycling, and the integration of materials in composite shells that reduces the diffusion path of energy carriers in a chemical reaction.^[17–19] So far developed functional hollow materials are efficient as energy conversion catalysts or anode materials near room

[✉] Muhammad Waqas

muhammad.waqas@kfupm.edu.sa

Interdisciplinary Research Center for Refining and Advanced Chemicals, King Fahd University of Petroleum & Minerals, Dhahran 31261, Saudi Arabia

temperature, but they are not stable as gas-phase tandem catalysis because of extreme conditions. Another example is the development of bi- and multi-functional tandem catalysis, which is an efficient process intensification technique for chemical processes. It involves combining numerous successive chemical reactions in a single vessel or catalyst under comparable or identical circumstances.^[20–22] To do this, metal oxide-zeolite bifunctional catalysts have been extensively investigated for assisting tandem reactions due to the diverse catalytic capabilities of MO and ZEO, which cover a broad range of chemical reactions.^[23–29] Currently, $\text{ZnCrO}_x/\text{H-MSAPO}$,^[30] $\text{Zn-ZrO}_2/\text{H-ZSM-5}$,^[31] $\text{In}_2\text{O}_3/\text{H-ZSM-5}$,^[32] and $\text{Cr}_2\text{O}_3/\text{H-ZSM-5}$ ^[33] were synthesized to directly convert syngas (a blend of CO and H₂) or CO₂ into valuable chemicals without the need to separate or purify the intermediates.

Typically, a metal oxide-zeolites catalyst is usually produced either by physically mixing metal oxide nanoparticles as dopants with the zeolite substrate,^[30–33] or by an impregnation process,^[34,35] resulting in an architecture, where metal oxide nanoparticles are dispersed randomly on the zeolite. As a result, the uneven distribution of metal oxides on zeolites catalyzed the conversions instantly rather than sequentially. Furthermore, the metal oxides and zeolites components typically catalyze the initial and subsequent reactions in the tandem catalysis process for converting syngas and CO₂,^[30,32] and the products created in the first stage on the metal oxide site may diffuse out without undergoing further reactions on the zeolite phase. Therefore, a random architecture is not optimal for achieving the highest efficiency and desired sequence in the tandem reaction. This article presents a versatile and straightforward methodology for synthesizing nickel oxide@cobalt oxide@zeolites hollow spheres with defined metal-zeolite spatial organization and a short diffusion pathway. The synthesis approach gives control over many structural factors and chemical compositions. The nickel oxide nanocrystal encapsulation into carbon spheres and cobalt ions and zeolites enrichment into the ultimate solid carbon spheres are studied, and the fundamental processes governing the self-assembly and hollowing behaviors are revealed. Owing to the unique core-shell arrangement and the cage-effect of the NiO@Co₃O₄@ZSM-5 hollow sphere, it is expected to be an effective and stable catalyst in multi-purpose industry applications particularly as gas-phase tandem catalysis processes to yield valuable chemicals.

2 Experimental

2.1 Chemicals

Glucose (C₆H₁₂O₆, 99.5%), nickel (II) chloride hexahydrate

(NiCl₂·6H₂O, 99.9%), cobalt (II) acetate tetrahydrate [Co(CH₃CO₂)₂·4H₂O], sodium oleate [CH₃(CH₂)₇CH=CH-(CH₂)₇COONa, 99%], oleic acid (OA, C₉H₁₈C₈H₁₅-COOH, 99%), octadecane (99%), tetraethoxysilane [Si(OC₂H₅)₄, 98%], aluminium iso-propoxide (AIP, Al[OCH(CH₃)₃], 98%), tetrapropylammonium hydroxide [(CH₃CH₂CH₂)₄N(OH), TPAOH, 40% aq.], dodecyltrimethylammonium bromide (DTAB) and solvents, such as ethanol (95%), hexanes (85%), acetone (99.78%) were purchased from Sigma Aldrich and used as received unless mentioned.

2.2 Synthesis of Carbon Spheres

The carbon spheres (CSs) with rich surface hydrophilic moieties, such as carbonyl [(C=O), hydroxyl (C—OH), and carboxylic (COOH)] were synthesized according to our previously reported method with slight modification.^[9] Typically, 1.8 mol/L aqueous glucose solution was sealed into the Teflon lined, stainless steel autoclave and heated in the oven at 180 °C for 18 h. After the reaction, the reaction vessel was cooled down overnight. The CSs were centrifuged and washed with distilled water, ethanol, and acetone, respectively.

2.3 Synthesis of Nickel Oleate Complex and Nickel Oxide Nanocrystals

All the glassware has been cleaned thoroughly with aqua regia, rinsed with distilled water and dried at 120 °C to guarantee a clean glass surface. The nickel oleate complex was synthesized by using a published procedure with slight modification.^[36] Typically, in a flask round bottom three-neck, 4.8 g of nickel (II) chloride hexahydrate (20 mmol), 30 mL of distilled water, 12.29 g of sodium oleate (20 mmol), 40 mL of ethanol, and 70 mL of hexane were mixed and heated at 70 °C under constant stirred for 4 h. Then separating funnel was used to collect the greenish organic layer containing nickel oleate. The product was washed twice with distilled water, ethanol and twice with acetone to remove excessive oleic acid. Next, the hexane was evaporated with a rotary pump and the resultant nickel oleate complex was placed at room temperature for 12 h.

The synthesis of nickel oxide nanocrystals was carried out in a flask round bottom three-neck. The as-synthesized 12.8 g of nickel oleate (20.5 mmol), 3.26 mL of oleic acid (10.25 mmol) and 98 g of octadecane were combined and programmed heat at 3.3 °C per minute under stirring. Set the temperature at 320 °C, and keep refluxing for 30 min. When the solution temperature reached to 320 °C, the initial greenish color turned black. Then, the reaction flask was cool down at 50 °C and NiO-NCs were precipitated with 10 mL

of hexane and 40 mL of acetone. The NiO-NCs were washed with a mixture of hexane and acetone and centrifuged at the speed of 11000 r/min. The resultant NiO-NCs were dissolved in chloroform for long-term storage.

2.4 Self-assembly of NiO-NCs and Formation of NiO@CSs

The NiO-NCs were assembled in the oil and water microemulsion system. In a typical experiment, 100 mg of NiO-NCs were dispersed in 7.4 g of chloroform and added dropwise to 100 mg of DTAB in 10 g of distilled water and stirred overnight at 20 °C to evaporate chloroform. The excess DTAB was washed with distilled water in several cycles of centrifugation. The as-collected NiO-NCs/DTAB were dispersed in 1.8 mol/L aqueous glucose solution, sealed in Teflon lined, stainless steel autoclave and heated in the oven at 180 °C for 5 h. The NiO@CSs were centrifuged and washed with distilled water, ethanol, and acetone, respectively.

2.5 Synthesis of NiO@CSs-Co²⁺

Typically, for synthesizing NiO@CSs-Co²⁺, 1 mol/L of Co(CH₃COO)₂·4H₂O was adsorbed onto the freshly prepared 0.6 g of CSs dispersed in 30 mL of distilled water, sonicated for 15 min and aged for 6 h at room temperature followed by rinsing and drying.

2.6 Synthesis of Zeolite Nanocrystals

Zeolites nanocrystals; ZSM-5 (ZEO) with Si/Al=100 were synthesized by a reported method with some modifications.^[37,38] Typically, aluminium isopropoxide (AIP) and tetrapropylammonium hydroxide (TPAOH, 1 mol/L in H₂O) were transferred to a polypropylene bottle and stirred for 1 h at room temperature to get a clear solution. Afterwards, tetraethoxysilane (TEOS) and distilled water were added to the solution and stirred vigorously for 2 h at room temperature to hydrolyze the TEOS. The molarity of the composed solution at pH *ca.* 11.4 was 1 SiO₂/0.01 AIP/0.25 TPAOH/4 EtOH/20 H₂O. Then, the clear sol was heated at 80 °C under constant stirring to evaporate certain water contents until the molar ratio of H₂O/SiO₂ in the sol reached about 4.20. The resultant concentrated sol was transferred to a Teflon-lined stainless-steel autoclave for the hydrothermal treatment at 180 °C for 90 min. The hydrous zeolite nanocrystals (ZEO-NCs) were washed with distilled water 3-times and collected using centrifugation at a speed of 12000 r/min and 1 g of them were dispersed in 99 mL of distilled water to produce a *ca.* 1% (molar fraction) stable aqueous suspension.

2.7 Synthesis of NiO@Co₃O₄@ZEO Hollow Spheres

A specific volume (3 mL) of 1% (molar fraction) ZEO nanocrystal suspension was gradually added to an aqueous Co²⁺-CSs (1 mg/mL) solution while stirring in order to produce typical NiO@Co₃O₄@ZEO hollow spheres. After 1 h of stirring, the aqueous suspension was centrifuged at 2000 r/min for 5 min in order to extract the loose ZEO nanocrystals. NiO@CSs-Co²⁺@ZEO colloidal particles were then calcined in air at 500 °C for 3 h with a ramping rate of 6 °C/min to yield NiO@Co₃O₄@ZEO hollow spheres.

2.8 Characterization Methods

Scanning electron microscopy (SEM) images of the prepared materials were taken using a Jeol JEM-7210F. The crystal phases were examined by X-ray diffraction (XRD) on a Rigaku diffractometer with a Cu K α radiation source ($\lambda=1.5406 \text{ \AA}$, $1 \text{ \AA}=0.1 \text{ nm}$). Nitrogen adsorption-desorption isotherms were obtained at 273 and 298 K on a Quantachrome® Autosorb IQ instrument. A JEOL JEM-2100F transmission electron microscope (TEM) operating at 200 kV was used to analyze the crystal sizes and shapes. The powdered samples were created by dispersing them in ethanol, subjecting them to sonication, and then depositing them onto a carbon film grid. The atomic percentage of the material was determined using an energy-dispersive X-ray fluorescence analyzer (XRF), the JEOL JSX 3201.

3 Results and Discussion

3.1 Synthesis of NiO@Co₃O₄@ZEO Hollow Spheres

In Fig. 1 (see detail in methods), the schematic illustration has shown that the synthesis protocol involves four key steps: i) the development of colloidal nickel oxide nanocrystals (NiO-NCs) assembly in an oil-in-water microemulsion system. Chloroform-dispersed NiO-NCs are emulsified with a deionized water solution of DTAB, ii) confinement of NiO-NCs in the core of carbon spheres (CSs), iii) sequential loading of cobalt cations and zeolites (ZEO) colloids onto NiO@CSs; iv) calcination of NiO@Co²⁺@CS@ZEO in air combusted the organic template to form NiO@Co₃O₄@ZEO hollow spheres.

The synthesis of size-controlled NiO-NCs is achieved *via* a general wet chemistry route. Briefly, NiO-NCs were prepared by thermal decomposition of metal oleate. Scanning electron microscope (SEM) images show the spherical *ca.* 17.5 nm NiO-NPs with a narrow size distribution

histogram measured from Image J software (Fig. 2A). The self-assembly of NiO-NCs was achieved using oil in a water microemulsion system. The chloroform-dispersed NiO-NCs

were poured into the distilled water containing dodecyltrimethylammonium bromide (DTAB) and upon evaporation of chloroform, the colloidal assemblies of NiO-NCs were produced. Fig. 2B shows the corresponding SEM image of NiO-NCs self-assembly manifest spherical shape with an average diameter of about 67.5 nm. The diameter of NiO-NCs self-assembly can be tuned by adjusting the NiO-NCs and DTAB concentration. In the Fig. 2C, SEM image shows that uniform and monodispersed CSs with a mean diameter of 670 nm are produced by hydrothermal carbonization of glucose. The confinement of NiO-NCs in the core of CSs is achieved by reacting DTAB-modified positively charged NPs with terminal hydroxyl species of glucose molecules in a hydrothermal reactor that proceeds the cross-linked emulsification polymerization reaction.

SEM image in Fig. 2D shows the unprecedented nucleation of carbon stacks onto NiO-NCs core with a mean diameter of 4500 nm compared to the original CSs diameter (*ca.* 670 nm) derived from hydrothermal carbonization of glucose. It is noted that the growth of carbon onto NiO-NCs core can be controlled by adjusting the concentration of glucose. The present developed synthesis for NiO@CSs is general and various transition metal oxides and metal sulphides NPs can be self-assembled and confined into the core of CSs. The NiO@CSs have rich hydroxyl species inherited from glucose terminal hydroxyl that facilitate the

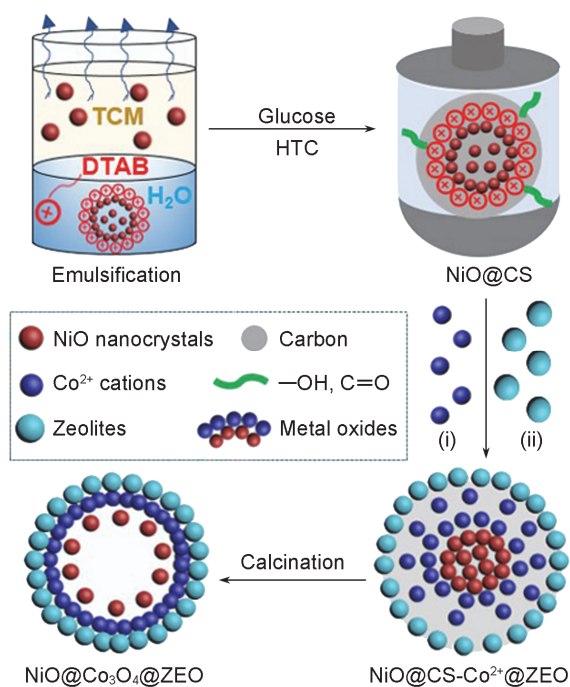


Fig. 1 Schematic illustration of the synthesis of NiO@Co₃O₄@ZEO hollow spheres

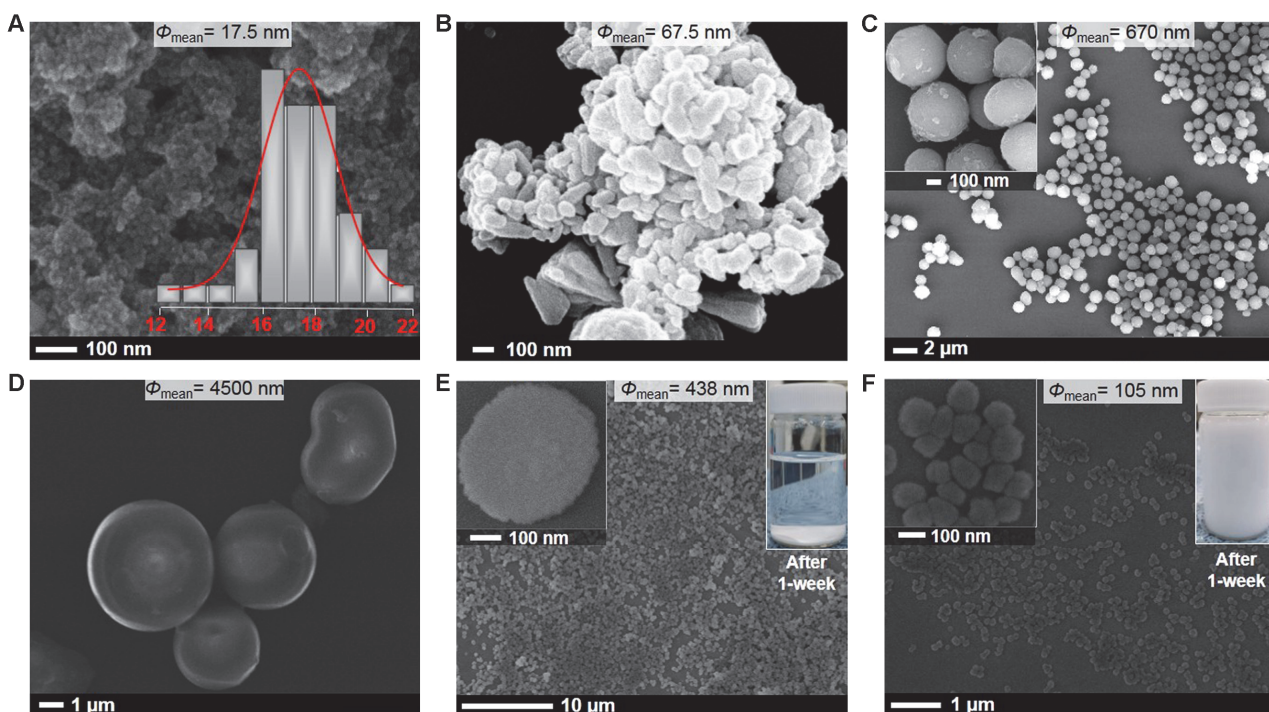


Fig. 2 SEM image of NiO nanocrystals (A) and particle size histogram analyzed by Image J (inset in A), SEM image of self-assembly of NiO nanocrystals (B), SEM image of CSs multiple particles (C) and enlarged particles (inset in C), SEM image of NiO@CSs(D), SEM image of ZEO multiple microcrystals (E) and that of single microcrystal (inset in left E) and 1% (mass fraction)solution image (inset in right E), and SEM image of multiple ZEO nanocrystals (F) and that of few ZEO nanocrystals (inset in left F) and 1% (mass fraction) solution image (inset in right F) with the symbol Φ_{mean} representing the average exterior diameter of the particle

electrostatic interaction to Co^{2+} cations to form NiO@CSs-Co^{2+} . Next, for making the zeolite shell onto NiO@CSs-Co^{2+} solid sphere, various sizes of ZEO-NCs are prepared by a hydrothermal method. For instance, SEM image in Fig. 2E shows the uniform ZEO microcrystals with a mean diameter of 438 nm whereas the inlet photograph is the 1% (mass fraction) ZEO microcrystal in distilled water. In Fig. 2F, SEM image shows the uniform ZEO-NCs with a mean diameter of 105 nm, whereas the inlet photograph is the 1% (mass fraction) ZEO-NCs suspension in water. Such highly dispersed and well-matched ZEO with notably small crystal size is crucial for uniform coating onto the outer surface of solid NiO@CSs-Co^{2+} .

3.2 Growth Mechanism for $\text{NiO@Co}_3\text{O}_4@\text{ZEO}$ Hollow Spheres

In water, the electrostatic attraction between positive charges and negative charges is readily comprehensible. Briefly, the NiO@CSs surface has abundant negative charges ($\text{C}=\text{O}$, $\text{C}-\text{OH}$) and micropores,^[5] when Co^{2+} cations and NiO@CSs are mixed in water, the Co^{2+} cations are evenly attached on the surface to form NiO@CSs-Co^{2+} solid sphere. Following, in water, the recognition force between ZEO and Co^{2+} is excluded because the NiO@CSs-M^{n+} (ζ -potential= -13.5 mV) and ZEO (ζ -potential= -14.4 mV) revealed that both material surfaces are negatively charged.^[39] Therefore, it is clear that the van der Waals interaction is accountable between NiO@CSs-Co^{2+} and ZEO-NCs and the Hamaker constant that measures the van der Waals forces^[40] is approx. an order of magnitude higher for NP@CSs-Co^{2+} . The high strength of Co^{2+} ions, 2 mol/L in solution, reduces the double layer repulsion and strengthens the van der Waals forces to induce aggression between ZEO-NCs and NiO@CS-Co^{2+} particles. Such van der Waals prompt aggression gives rise to excessive collision between the ZEO-NCs and NiO@CS-Co^{2+} particles and then hydrogen bonding plays its role in the aggression.^[41] Once, NiO@CS-Co^{2+} was stabilized by ZEO-NCs, colloidal assembly was restored and the aggregation was discontinued. In the SEM of Fig. 3A, a uniformed Co_3O_4 hollow sphere is synthesized

as a reference by loading Co^{2+} cations on CSs followed by annealing in air. Taking the synthesis of $\text{NiO@Co}_3\text{O}_4@\text{ZEO}$ hollow spheres as an example, NiO@CS@Co^{2+} and ZEO-NCs are mixed in water with stirring to form $\text{NiO@CS-Co}^{2+}@$ ZEO core-shell colloidal solid particles, in which ZEO-NCs are evenly adsorbed onto the surface of NiO@CS-Co^{2+} .

Further calcination of $\text{NiO@CS@Co}^{2+}@$ ZEO in air oxidatively decomposed the organic species and formed much smaller hollow $\text{NiO@Co}_3\text{O}_4@\text{ZEO}$ spheres (*ca.* 2800 nm) in place of original solid NiO@CSs (*ca.* 4500 nm). In the calcination, the combustion of carbonaceous and ammonium species does not impact on the material architecture. In Fig. 3B, the SEM image shows that the $\text{NiO@Co}_3\text{O}_4@\text{ZEO}$ hollow spheres are spherical particles and each particle is composed of a hollow $\text{NiO@Co}_3\text{O}_4$ core and a hollow ZSM-NCs shell. In Fig. 3C, the TEM image further confirms that the ZEO shell forms on the surface of $\text{NiO@Co}_3\text{O}_4$ whereas selective area electron diffraction (SAED) shows the amorphous nature of ZEO-NCs (inset top and bottom respectively).

Fig. 3D shows magnified TEM image of crystalline Co_3O_4 shell in $\text{NiO@Co}_3\text{O}_4@\text{ZEO}$ hollow spheres, which confirms a lattice plane spacing of 0.47 nm that aligns with (111) of cubic spinel Co_3O_4 , assuming that is among the exposed surfaces of the Co_3O_4 polyhedron (inset top). The

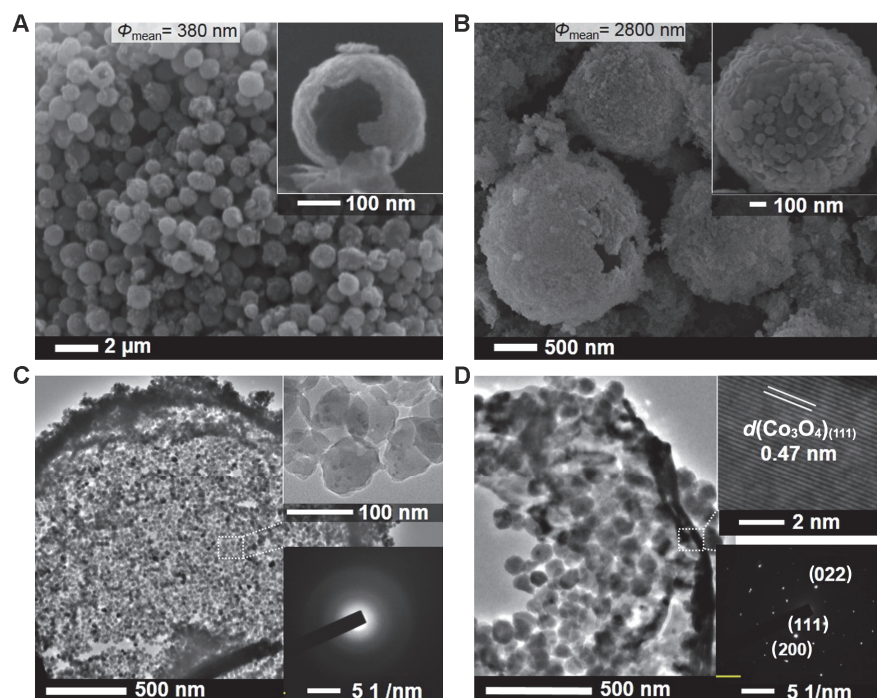


Fig. 3 SEM image of Co_3O_4 hollow spheres (A), SEM image of $\text{NiO@Co}_3\text{O}_4@\text{ZEO}$ hollow spheres (B), TEM image of $\text{NiO@Co}_3\text{O}_4@\text{ZEO}$ hollow spheres (C) and TEM image and SAED pattern of zeolite nanocrystals (inset top and bottom respectively in C), TEM image of magnified Co_3O_4 shell of $\text{NiO@Co}_3\text{O}_4@\text{ZEO}$ hollow spheres (D) and high-resolution TEM image and SAED pattern of Co_3O_4 (inset top and bottom respectively in D) with the symbol Φ_{mean} representing the average exterior diameter of the spherical particle

SAED pattern in Fig. 3D displays diffractions indexed to lattice planes (111), (022), and (200), corresponding to spacings of approximately 0.47, 0.286, and 0.404 nm,^[42] respectively.

In Fig. 4A, X-ray diffraction (XRD) was used to examine the crystalline structures of the synthesized Co_3O_4 hollow spheres. No further peaks were found, and all reflection peaks were indexed to a pure cubic spinel Co_3O_4 structure. In Fig. 4B, the $\text{NiO}@\text{Co}_3\text{O}_4@\text{ZEO}$ XRD patterns revealed the prominent peaks of ZSM-5, Co_3O_4 , and NiO nanoparticles in comparison to pure Co_3O_4 hollow spheres. As an impurity, extremely weak XRD peaks corresponding to Co_2SiO_4 were found. In Fig. 4C, the $\text{NiO}@\text{Co}_3\text{O}_4@\text{ZEO}$ has a Brunauer-Emmett-Teller specific surface area (S_{BET}) of 296.1 m²/g and micropores of 131 m²/g arising from the ZEO shell.

Fig. 5 shows a typical X-ray fluorescence spectrum of $\text{NiO}@\text{Co}_3\text{O}_4@\text{ZEO}$ hollow spheres. The noticeable peaks in the spectrum are the $K\alpha$ peaks for each of the sample primary

components. Table 1 summarizes the key components and elemental concentrations of the sample study.

Here, it is important to understand the hollowing mechanism: transformation from solid $\text{NiO}@\text{CSs-Co}^{2+}@\text{ZEO}$ to hollow $\text{NiO}@\text{Co}_3\text{O}_4@\text{ZEO}$ spheres. To do this CSs- Co^{2+} , solid sphere thermogravimetry analysis was determined to unfold the decomposition of carbonaceous species, and phase transition. In Fig. 6, the first significant mass loss is observed at 247 °C, this indicates that the gradual radial combustion of carbon species is initiated at the CSs' surface. The second sharp exothermic DTA peak appeared at 319 °C, indicating that the flow of heat radially diffused towards the carbon stacks of the core and transformed C to CO_2 . Since Co^{2+} ions are abundantly throughout the CSs, therefore, it is likely that in the temperature range of 247 °C to 319 °C, the combustion of carbon exposes the Co^{2+} ions to meet with the inward diffused oxygen anion and formed solid amorphous CoO_x core.

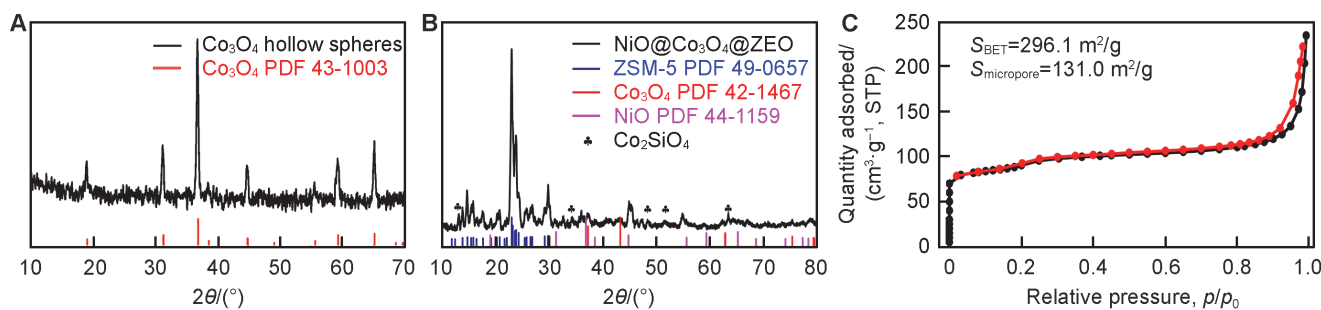


Fig. 4 X-Ray diffraction patterns of the as-synthesized Co_3O_4 hollow sphere (A), XRD patterns of $\text{NiO}@\text{Co}_3\text{O}_4@\text{ZEO}$ hollow spheres (B), and nitrogen adsorption-desorption isotherm of $\text{NiO}@\text{Co}_3\text{O}_4@\text{ZEO}$ hollow spheres (C) with the micropore area being calculated using the t-plot method

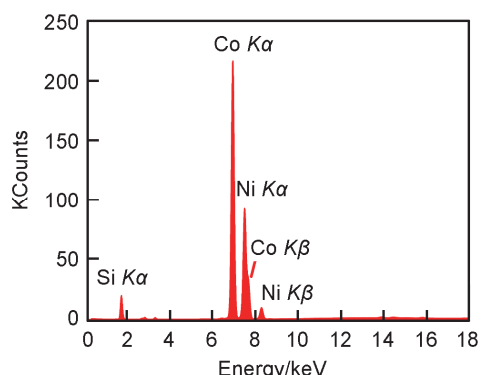


Fig. 5 X-Ray fluorescence spectrum of $\text{NiO}@\text{Co}_3\text{O}_4@\text{ZEO}$ hollow spheres

Table 1 X-Ray fluorescence (XRF) analysis of $\text{NiO}@\text{Co}_3\text{O}_4@\text{ZEO}$ hollow spheres containing the approximate concentration of elements

Element	Ni	Co	Si	Al	Sum
wt. (%)	4.70	13.38	23.05	0.067	41.21
Normalized wt. (%)	11.4	32.47	55.95	0.164	100
Normalized atomic fraction (%)	7.08	20.08	72.60	0.22	100

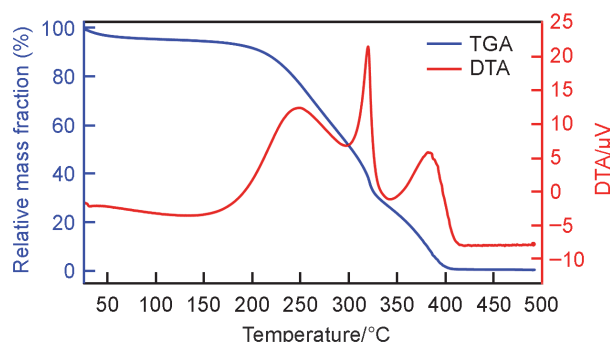


Fig. 6 TGA and DTA cures for Co_3O_4 hollow spheres

Experiment is conducted under an air atmosphere to exactly replicate the standard synthetic conditions.

The complete mass loss of carbon species is observed at 412 °C, it is expected that the solid amorphous CoO_x core is saturated with the excessive oxygen contents resultantly, transformed into denser and hollower spheres. It is noteworthy that at 412 °C, the Co_3O_4 particles near the surface of spheres are likely to be more crystalline and those residing in the interior are amorphous. Therefore, further increasing the temperature from 412 °C to 500 °C and holding for 3 h ensures that each Co_3O_4 particle saturates

with atmospheric oxygen, leading to inducing the crystallinity to the whole sphere. From the TEM image in Fig. 3, C and D, it is clear that the interior of the NiO@Co₃O₄@ZEO is hollow. Also, the Co₃O₄ particles have notably higher density in shells with uniform inter-shell voids. It is well established that the crystalline phase usually has a high density compared to the amorphous phase. So, hollowing the shells involves the simultaneous occurrence of inward crystallization and outward contraction, leading to gradual hollowing from the center. This is comparable with the Kirkendall effect,^[43] in which two different materials/phases have differing inter-diffusion rates, resulting in both boundary motion and vacancy enrichment. Here, the phase transition from kinetically unstable amorphous to stable crystalline is based on the dissolution and recrystallization of the amorphous phase, exhibiting the features of Ostwald ripening growth.^[44] Thus, it is a fair inference that the hollowing process may involve both Kirkendall and Ostwald ripening mechanisms.

4 Conclusions

The present study introduces an innovative arrangement of multi-site metal oxide-zeolite hollow structures in comparison to conventional approaches. The synthesis is ubiquitous, showcasing tunable structural features and chemical compositions. The systematic disclosure of nanocrystal assembly, material growth, and hollowing mechanism advances the understanding of rational integration of selected materials in core-shell or multiple-shelled hollow spheres, which is useful in a wide range of gas-phase catalytic processes and beyond.

Acknowledgements

The authors would like to express their gratitude to the King Fahd University of Petroleum & Minerals (KFUPM), located in Dhahran, Saudi Arabia, for the support that they have provided.

Conflicts of Interest

The authors declare no conflicts of interest.

References

- [1] Wei Y., Li J., Zhao D., Zhao Y., Zhang Q., Gu L., Wan J., Wang D., *CCS Chemistry*, **2024**, 6, 1.
- [2] Wei Y., Zhao D., Wang D., *Adv. Sci.*, **2023**, 11, 2305408.
- [3] Ge W., Chen X., Ma R., Zheng S., Shang N., Zhao X., *Chem. Res. Chinese Universities*, **2024**, 40, 1.
- [4] Waqas M., Ahmad H., *Chemosphere*, **2024**, 350, 140968.
- [5] Waqas M., *Inorg. Chem.*, **2021**, 60, 13461.
- [6] Zhao X., Yang M., Wang J., Wang D., *Chem. Res. Chinese Universities*, **2023**, 39, 630.
- [7] Waqas M., Iqbal S., Bahadur A., Saeed A., Raheel M., Javed M., *Appl. Catal. B: Environ.*, **2017**, 219, 30.
- [8] Waqas M., Yang B., Cao L., Zhao X., Iqbal W., Xiao K., Zhu C., Zhang J., *Catal. Sci. & Technol.*, **2019**, 9, 5322.
- [9] Waqas M., Wei Y., Mao D., Qi J., Yang Y., Wang B., Wang D., *Nano Res.*, **2017**, 10, 3920.
- [10] Xu W., Bi R., Yang M., Wang J., Yu R., Wang D., *Nano Res.*, **2023**, 16, 12745.
- [11] Mao D., Zhang Z., Yang M., Wang Z., Wang D., *Int. J. Miner. Metall. Mater.*, **2023**, 30, 581.
- [12] Han W., Wei Y., Wan J., Nakagawa N., Wang D., *Inorg. Chem.*, **2022**, 61, 5397.
- [13] Wei Y., Wan J., Wang J., Zhang X., Yu R., Yang N., Wang D., *Small*, **2021**, 17, 2005345.
- [14] Wang D., Wang H., Qi J., Yang N., Cui W., Wang J., Li Q., Yu X., Gu L., Yu R., Huang K., Feng S., Song S., Li J., *Angew. Chem. Int. Ed.*, **2020**, 59, 19691.
- [15] Zhang H., Zhang S., Guo B., Yu L.-J., Ma L., Hou B., Liu H., Zhang S., Wang J., Song J., Tang Y., Zhao X., *Angew. Chem. Int. Ed.*, **2024**, n/a: e202400285.
- [16] Ma L., Hou B., Zhang H., Yuan S., Zhao B., Liu Y., Qi X., Liu H., Zhang S., Song J., Zhao X., *Chem. Eng. J.*, **2023**, 453, 139735.
- [17] Wang J., Yang N., Tang H., Dong Z., Jin Q., Yang M., Kisailus D., Zhao H., Tang Z., Wang D., *Angew. Chem. Int. Ed.*, **2013**, 52, 6417.
- [18] Qi J., Zhao K., Li G., Gao Y., Zhao H., Yu R., Tang Z., *Nanoscale*, **2014**, 6, 4072.
- [19] Zhou B., Waqas M., Yang B., Xiao K., Wang S., Zhu C., Li J., Zhang J., *App. Surf. Sci.*, **2020**, 506, 145004.
- [20] Climent M. J., Corma A., Iborra S., Sabater M. J., *ACS Catal.*, **2014**, 4, 870.
- [21] Behr A., Vorholt A. J., Ostrowski K. A., Seidensticker T., *Green Chem.*, **2014**, 16, 982.
- [22] Lohr T. L., Marks T. J., *Nat. Chem.*, **2015**, 7, 477.
- [23] Védrine J. C., *ChemSusChem*, **2019**, 12, 577.
- [24] de Jong K. P., *Synthesis of solid catalysts John Wiley & Sons*, **2009**.
- [25] Chen S., Takata T., Domen K., *Nat. Rev. Mater.*, **2017**, 2, 1.
- [26] Hong W. T., Risch M., Stoerzinger K. A., Grimaud A., Suntivich J., Shao-Horn Y., *Energy & Environ. Sci.*, **2015**, 8, 1404.
- [27] Corma A., *Chem. Rev.*, **1997**, 97, 2373.
- [28] Vogt E. T. C., Weckhuysen B. M., *Chem. Soc. Rev.*, **2015**, 44, 7342.
- [29] Li Y., Li L., Yu J., *Chem.*, **2017**, 3, 928.
- [30] Jiao F., Li J., Pan X., Xiao J., Li H., Ma H., Wei M., Pan Y., Zhou Z., Li M., Miao S., Li J., Zhu Y., Xiao D., He T., Yang J., Qi F., Fu Q., Bao X., *Science*, **2016**, 351, 1065.
- [31] Cheng K., Zhou W., Kang J., He S., Shi S., Zhang Q., Pan Y., Wen W., Wang Y., *Chem.*, **2017**, 3, 334.
- [32] Gao P., Li S., Bu X., Dang S., Liu Z., Wang H., Zhong L., Qiu M., Yang C., Cai J., Wei W., Sun Y., *Nat. Chem.*, **2017**, 9, 1019.
- [33] Wang Y., Tan L., Tan M., Zhang P., Fang Y., Yoneyama Y., Yang G., Tsubaki N., *ACS Catal.*, **2019**, 9, 895.
- [34] Takeuchi M., Kimura T., Hidaka M., Rakhamawaty D., Anpo M., *J. Catal.*, **2007**, 246, 235.
- [35] Huang H., Huang H., Feng Q., Liu G., Zhan Y., Wu M., Lu H., Shu Y., Leung D. Y. C., *Appl. Catal. B: Environ.*, **2017**, 203, 870.
- [36] Bronstein L. M., Huang X., Retrum J., Schmucker A., Pink M., Stein B. D., Dragnea B., *Chem. Mater.*, **2007**, 19, 3624.
- [37] Selvin R., Hsu H.-L., Roselin L. S., Bououdina M., *Synth. React. Inorg. M.*, **2011**, 41, 1028.
- [38] Roselin L. S., Selvin R., Bououdina M., *Chem. Eng. Commun.*, **2012**, 199, 221.
- [39] Xiao J., Cheng K., Xie X., Wang M., Xing S., Liu Y., Hartman T., Fu D., Bossers K., van Huis MA., *Nat. Mater.*, **2022**, 21, 572.
- [40] Israelachvili J. N., *Intermolecular and Surface Forces, 3rd Edition*, Waltham, MA: San Diego, CA, **2011**.
- [41] Lee J. S., Kim J. H., Lee Y. J., Jeong N. C., Yoon K. B., *Angew. Chem. Int. Ed.*, **2007**, 46, 3087.
- [42] Guo R., Wang R., Ni Z., Liu X., *Appl. Phys. A*, **2018**, 124, 623.
- [43] Yin Y., Rioux R. M., Erdonnez C. K., Hughes S., Somorjai G. A., Alivisatos A. P., *Science*, **2004**, 304, 711.
- [44] Cao L., Chen D., Caruso R. A., *Angew. Chem. Int. Ed.*, **2013**, 52, 10986.